

# Core-Collapse Supernovae: Modeling between Pragmatism and Perfectionism

*H.-Th. Janka, R. Buras, F.S. Kitaura Joyanes, A. Marek, and M. Rampp*

*Max-Planck-Institut für Astrophysik, Karl-Schwarzschild-Str. 1, D-85741 Garching, Germany*

## Abstract

We briefly summarize recent efforts in Garching for modeling stellar core collapse and post-bounce evolution in one and two dimensions. The transport of neutrinos of all flavors is treated by iteratively solving the coupled system of frequency-dependent moment equations together with a model Boltzmann equation which provides the closure. A variety of progenitor stars, different nuclear equations of state, stellar rotation, and global asymmetries due to large-mode hydrodynamic instabilities have been investigated to ascertain the road to finally successful, convectively supported neutrino-driven explosions.

## 1 Methods

Our neutrino-hydrodynamic simulations were performed with a conservative, high-resolution shock-capturing scheme that employs an exact Riemann solver and integrates the hydrodynamics equations with third order accuracy in space and second order accuracy in time. This code is coupled to a neutrino transport scheme that solves the energy-dependent moment equations of neutrino number, energy, and momentum of order  $(v/c)$  by making use of a variable Eddington factor closure which is calculated from a model Boltzmann equation [1]. In addition to radial derivatives, the moment equations are supplemented by  $(v_\theta)$ -dependent terms that correspond to the advection of neutrinos with fluid motions in lateral direction (with  $v_\theta$  being the lateral component of the velocity vector in spherical coordinates), and the equation of motion of the stellar plasma contains also lateral gradients of the neutrino pressure [2]. General relativistic effects are taken into account approximately by (i) a generalized gravitational potential (the radial part of which is constructed by a comparison with the Tolman-Oppenheimer-Volkoff equation, including terms due to fluid motion and neutrino effects) and (ii) relativistic redshift terms in the transport equations [1]. A comparison with a fully relativistic treatment in spherical symmetry yields very satisfactory results [3]. We have continuously modernized our treatment of neutrino interactions in the supernova medium, now including a variety of reactions and improvements (e.g., nucleon-nucleon bremsstrahlung; interactions between neutrinos of different flavors; correlations, weak magnetism and recoil in neutrino-nucleon interactions; electron captures on heavy nuclei according to recent calculations by Langanke and coworkers) in extension to the standard treatment of neutrino-matter interactions in supernova simulations (see Refs. [1, 2, 4] and the references to a long list of original papers therein).

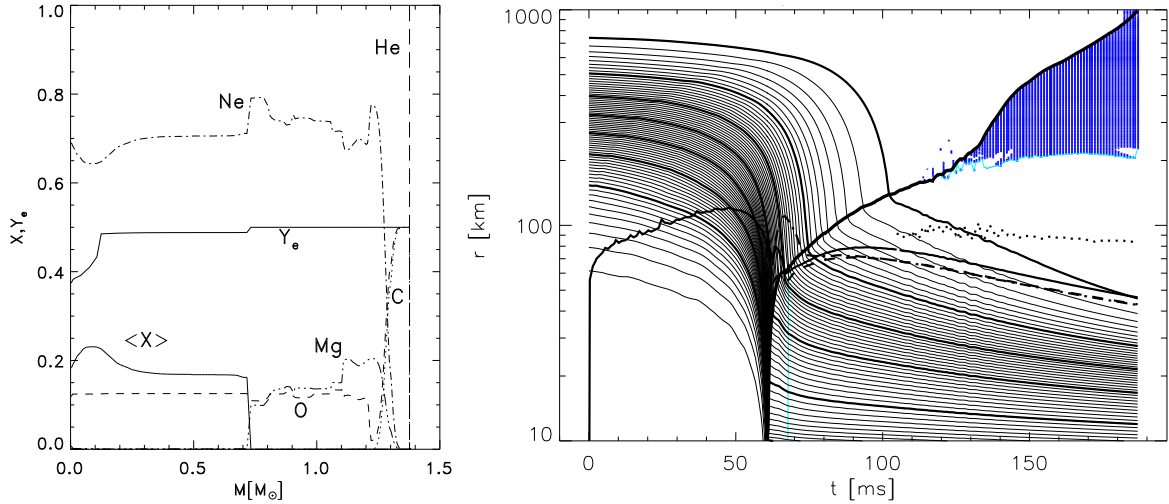


Figure 1: *Left:* Composition in the highly degenerate  $1.38 M_\odot$  core of an  $8\text{--}10 M_\odot$  progenitor [6] with O, Ne and Mg in the central region enclosed by an C-O shell.  $\langle X \rangle$  denotes the mass fraction of a representative neutron-rich heavy nucleus that appears in nuclear statistical equilibrium, and  $Y_e$  is the electron fraction. *Right:* Mass trajectories, shock position (thick solid line that rises to the upper right corner of the plot, where it reaches the surface of the C-O shell), and neutrinospheres ( $\nu_e$ : solid;  $\bar{\nu}_e$ : dash-dotted;  $\nu_\mu, \bar{\nu}_\mu, \nu_\tau, \bar{\nu}_\tau$ : dashed), and gain radius (dotted) for the collapsing O-Ne-Mg core. The mass trajectories are equidistantly spaced with intervals of  $0.01 M_\odot$ . The (blue) hatched region is characterized by a dominant mass fraction of He. (The plots were taken from Ref. [7].)

## 2 Results

In the past two years we have applied our new neutrino-hydrodynamics code to core-collapse simulations in one and two dimensions for a broad variety of progenitors, spanning the range from O-Ne-Mg cores on the low-mass end ( $\sim 8\text{--}10 M_\odot$ ) to  $25 M_\odot$  on the high-mass side. We have investigated different input for neutrino-matter interactions and have recently also tested the effects of different nuclear equations of state. This work was mostly done in course of the PhD Thesis of R. Buras and the Diploma Theses of F.S. Kitaura Joyanes and A. Marek. Below some main results are briefly summarized.

### 2.1 Explosion of an O-Ne-Mg core

The main improvement of our new simulations of O-Ne-Mg core collapse — which we did so far only in spherical symmetry — compared to previous approaches is the more accurate treatment of neutrino transport and neutrino-matter interactions. Using the nuclear equation of state (EoS) of Ref. [5], we could not confirm [7] that a prompt explosion occurs as found in calculations with simpler neutrino treatment but also with a different EoS [8]. The shock is created at a mass coordinate of  $\sim 0.45 M_\odot$  (defined by the moment when the postshock entropy first exceeds  $3 k_B$  per nucleon) and stalls (defined by the time when the postshock velocity becomes negative) only 1.2 ms later at  $\sim 0.8 M_\odot$ , still well inside the neutrinosphere and *before* energy losses by the prompt  $\nu_e$  burst could have contributed to its damping. We also do not find the powerful shock revival by neutrino heating as seen in Ref. [9] (cf. also Ref. [10]). Instead, the shock continuously expands due to the monotonically decreasing preshock density associated with the steeply dropping density at the interface between C-O

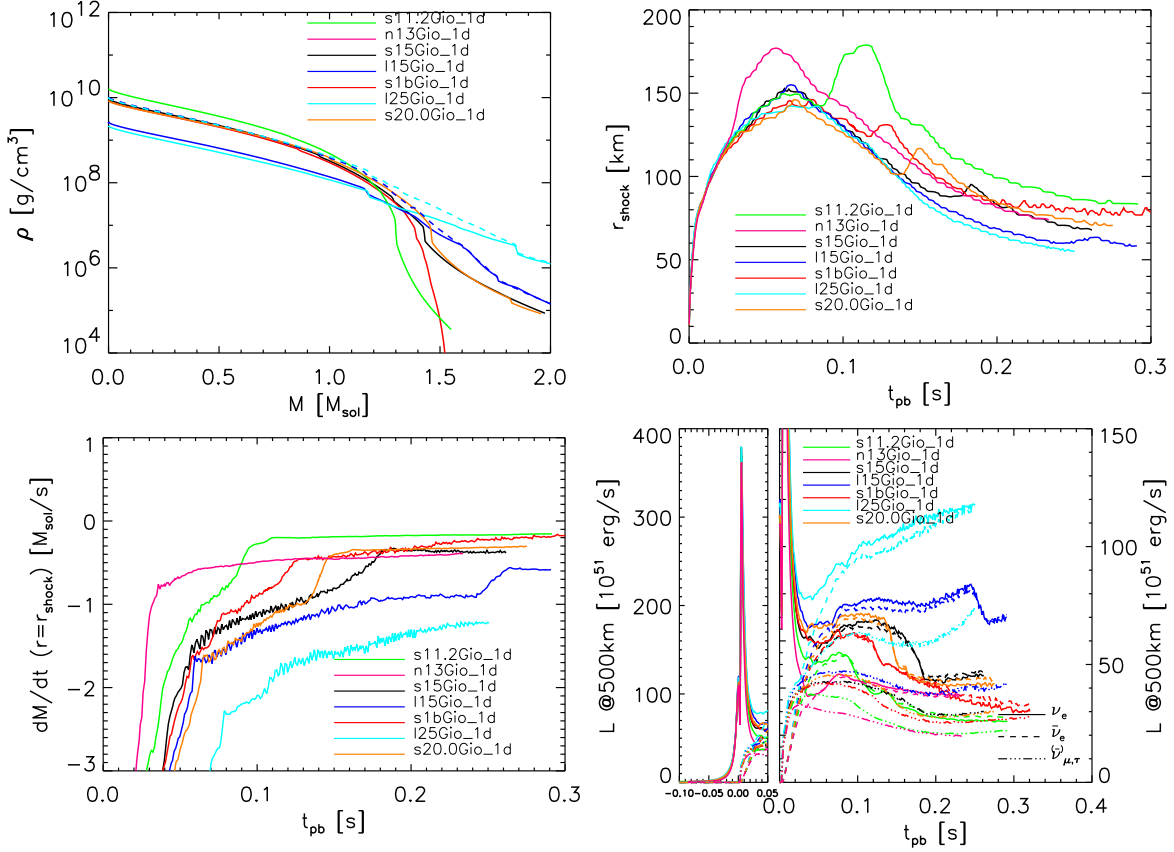


Figure 2: *Top left*: Density profiles of a sample of progenitor cores for stars with main sequence masses between  $11.2 M_{\odot}$  and  $25 M_{\odot}$  according to Ref. [13] ( $13 M_{\odot}$ , n13Gio\_1d), Ref. [14] ( $11.2$ ,  $15$ ,  $20 M_{\odot}$ , s11.2Gio\_1d, s15Gio\_1d, s20.0Gio\_1d, respectively), Ref. [15] (a Type Ib progenitor, s1bGio\_1d), and Ref. [16] ( $15$  and  $25 M_{\odot}$ , l15Gio\_1d and l25Gio\_1d, respectively). The dashed lines show profiles of the latter models after we have evolved them to a central density similar to that of the other progenitors. *Top right*: Shock positions vs. time for the set of progenitors. No explosions were obtained in spherical symmetry. *Bottom left*: Mass accretion rates by the shock as functions of time. The steep density gradients at composition interfaces cause sudden drops of  $|\dot{M}|$ . *Bottom right*: Luminosities of  $\nu_e$  (solid lines),  $\bar{\nu}_e$  (dashed) and heavy-lepton  $\nu$ 's and  $\bar{\nu}$ 's (dash-dotted), measured by a comoving observer at 500 km, around the prompt  $\nu_e$  burst (left panel) and during the post-bounce evolution (right panel).

shell and He shell (Fig. 1). Towards the end of our simulation the mass accretion rate by the shock has correspondingly dropped to less than  $0.03 M_{\odot} s^{-1}$ . Although our simulation is not yet finally conclusive in this point, we see indications that a neutrino-driven wind begins to fill the volume between neutron star surface and shock and will lead to mass ejection with a rather low “explosion” energy and little Ni production, very similar to the outcome of simulations of accretion induced white dwarf collapse to neutron stars [11]. But the results of O-Ne-Mg core collapse can be sensitive to the properties of the nuclear EoS [12]. We plan to investigate this in future simulations.

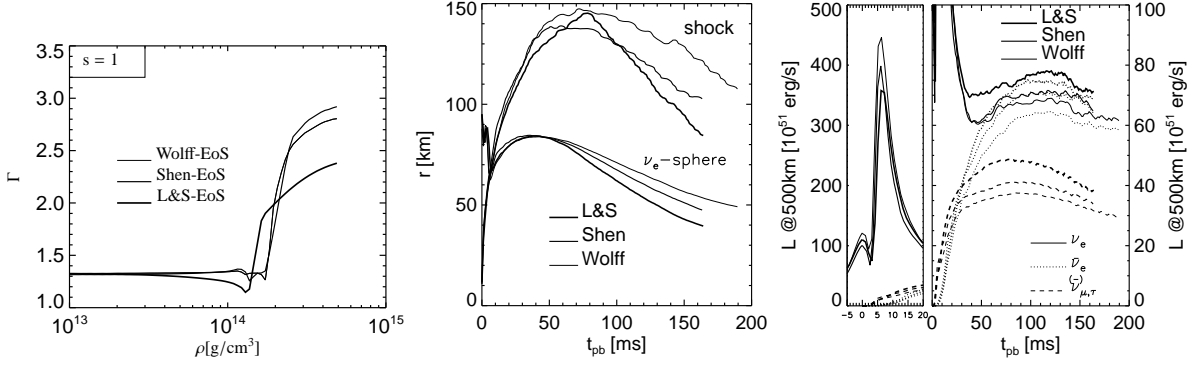


Figure 3: *Left:* Adiabatic index  $\Gamma \equiv (d \ln P / d \ln \rho)_s$  for an entropy  $s = 1 k_B$  per nucleon (and an electron fraction  $Y_e = 0.4$ ) for the equations of state of Ref. [8] (“Wolff”, thin lines), Ref. [23] (“Shen”, medium) and Ref. [5] (“L&S”, thick). *Middle:* Shock positions and neutrinospheric radii of  $\nu_e$  as functions of time for collapse simulations of a  $15 M_\odot$  progenitor (Model s15a28 [20]) with the three nuclear equations of state. *Right:* Prompt  $\nu_e$  burst (left panel) and post-bounce luminosities of  $\nu_e$  (solid lines),  $\bar{\nu}_e$  (dotted) and heavy-lepton  $\nu$ 's and  $\bar{\nu}$ 's (dashed) for the core collapse simulations of the  $15 M_\odot$  star with the three different equations of state. (The plots were taken from Ref. [24].)

## 2.2 One-dimensional core collapse for progenitors between $11 M_\odot$ and $25 M_\odot$

In spherical symmetry none of the investigated core collapse models, all evolved with the EoS of Lattimer and Swesty [5], developed an explosion until we stopped the simulations at typically 300 ms after bounce. This confirms the results of fully relativistic simulations by Liebendörfer et al. [17]. In spite of a rapidly dropping rate of mass accretion through the shock (Fig. 2) neutrino heating is not strong enough to reverse the postshock infall of the accreted matter, and the shock retreats in all cases, following the contraction of the neutrinosphere, after it had temporarily expanded to a maximum radius between 140 km and 180 km (Fig. 2). The latter expansion was driven by the accumulation of accreted matter between shock and neutrinosphere during the early post-bounce phase when the accretion rate is very high. The bumps visible in the shock trajectories (Fig. 2) correspond to the density and entropy discontinuities at the interfaces between shells of different composition, where the shock experiences a sudden drop of the mass accretion rate. Note the astonishing similarity of the prompt  $\nu_e$  burst, which is a consequence of the very similar structure of the inner  $\sim 1 M_\odot$  of the Fe core for different progenitors before collapse (Fig. 2) and the fact that the structural similarity is still present at bounce. The large luminosity differences during the post-bounce evolution are caused by model-to-model variations of the structure near and beyond the outer edge of the iron core (cf. also [18]). First core-collapse simulations of  $15 M_\odot$  and  $25 M_\odot$  progenitors with electron captures on heavy nuclei being treated according to Ref. [19] suggest that these findings also apply when electron captures on nuclei instead of free protons dominate during the infall phase.

## 2.3 Variations of the nuclear equation of state

For a  $15 M_\odot$  progenitor (Model s15a28 [20]) we have investigated the influence of the nuclear EoS on core collapse, shock formation, and post-bounce evolution in three different cases. We ran simulations with

- (i) our standard EoS (Lattimer and Swesty, “L&S”) [5], which is based on a compressible

liquid drop model and employs a Skyrme force for the nucleon interaction (our choice of the compressibility modulus of bulk nuclear matter is 180 MeV, and the symmetry energy parameter 29.3 MeV, but the differences in the supernova evolution caused by other values of the compressibility were shown to be minor [21, 22]);

(ii) a new relativistic mean field EoS (Shen et al., “Shen”) [23] with a compressibility of nuclear matter of 281 MeV and a symmetry energy of 36.9 MeV;

(iii) an EoS that was constructed by Hartree-Fock calculations with a Skyrme force for the nucleon-nucleon interaction (Wolff and Hillebrandt, “Wolff”) [8] and has a compressibility of 263 MeV and a symmetry energy of 32.9 MeV.

The three equations of state show, for example, clear differences in the adiabatic index  $\Gamma \equiv (d \ln P / d \ln \rho)_s$  around and above the phase transition to homogeneous nuclear matter (Fig. 3).

Significant differences were also found during the core-collapse calculations:

- (a) in the nuclear composition of the progenitor core and during infall;
- (b) in the maximum density reached at bounce, and the density in hydrostatic equilibrium afterwards;
- (c) in the shock formation point, which is shifted outward by  $\sim 0.05 M_\odot$  in case of the stiffer Wolff and Shen EoSs [23, 8];
- (d) in the shock stagnation point (defined by the time when the postshock velocities start to become negative), which moves out by up to  $\sim 0.1 M_\odot$  (or  $\sim 10$  km) for the stiffer EoSs;
- (e) concerning the existence and duration of a post-bounce phase where a shell with a sizable mass fraction of heavy nuclei occurs transiently outside of the nuclear core;
- (f) in the radius of maximum shock expansion and subsequent shock contraction, which closely follows the contraction behavior of the nascent neutron star (Fig. 3);
- (g) in the peak luminosity during the prompt  $\nu_e$  burst and the evolution of the post-bounce neutrino luminosities (Fig. 3);
- (h) despite of differences in details, an application of the Ledoux criterion suggests a qualitatively similar behavior of convectively unstable regions in the neutron star and in the neutrino-heating layer.

The publication of a detailed discussion of these results is in preparation (Marek et al. 2004).

## 2.4 Two-dimensional models

Convective overturn in the neutrino-heated postshock layer plays an important role during the supernova evolution and can provide the crucial push for delayed shock revival by an enhancement of the efficiency of neutrino energy transfer [25, 26, 27]. This is also seen in our recent simulations which employ a much improved treatment of neutrino transport compared to previous models. Although we found convective enhancement of shock expansion [28], we were, however, not able to confirm the successful explosions obtained in simulations with considerable approximations of the neutrino physics [29].

Rotation of the Fe core of the progenitor star, even at a moderate rate, supports strong postshock convection and brings the star much closer to an explosion by the neutrino-heating mechanism. In a simulation of a  $15 M_\odot$  progenitor we assumed the Fe core to rotate rigidly with a rate of  $\Omega = 0.5 \text{ rad s}^{-1}$  [28, 30], which is in the ballpark of results from stellar evolution calculations [31] and significantly slower than adopted in other recent works (e.g., by Burrows and collaborators [32] and Kotake et al. [33], see also their contributions to this meeting). Our rotating model showed shock expansion to a maximum radius of nearly 300 km along

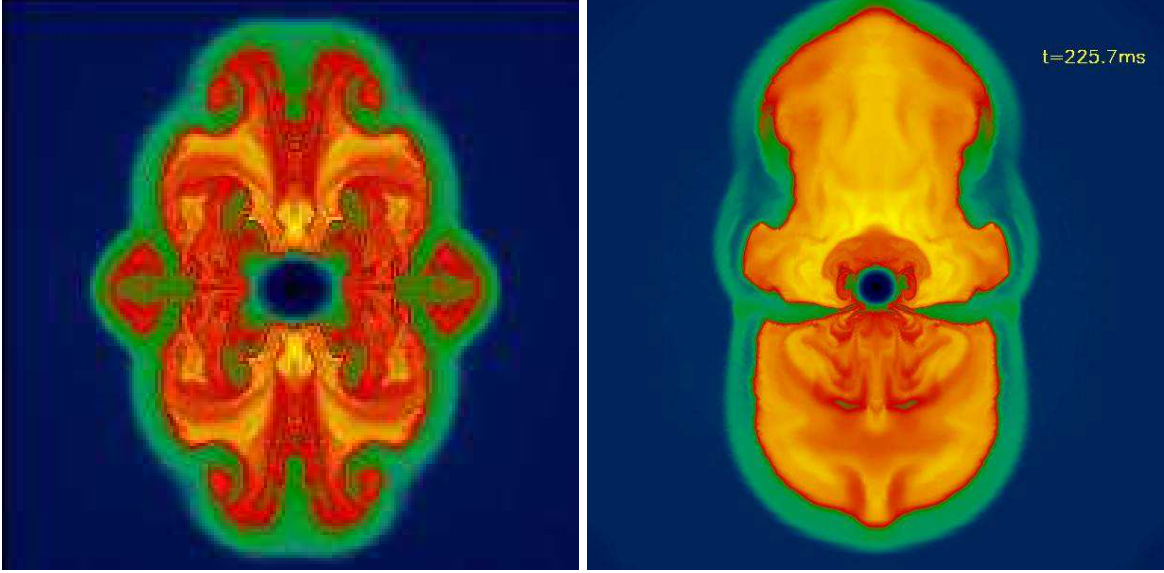


Figure 4: Snapshots of the entropy distribution at  $t > 200$  ms post bounce for two two-dimensional simulations with “Boltzmann neutrino transport” as described in Sect. 1. Yellow denotes highest entropies (around  $15\text{--}25 k_B$  per nucleon), red, green, and blue ( $\lesssim 8 k_B$  per nucleon) successively lower values. *Left*: Result at 245 ms p.b. for a  $15 M_\odot$  progenitor whose Fe core was assumed to rotate rigidly with  $\Omega = 0.5 \text{ rad s}^{-1}$  [28, 30], which is in the ballpark of predictions from stellar evolution models [31]. Equatorial symmetry was assumed. At the displayed time the shock reaches its largest expansion of nearly 300 km in the axial (in the plot vertical) direction, but later on contracts again. *Right*: Situation in an  $11.2 M_\odot$  star at 226 ms post bounce (when the simulation had to be stopped because of shortage of computer time) [36]. The shock has reached a maximum radius of 600 km with no sign of return. Global, violent low-mode bipolar oscillations of the postshock layer, which were possible in this simulation due to a  $180^\circ$  grid, support a weak explosion in this *nonrotating* model. Note the significant polar to equatorial deformation.

the rotation axis (Fig. 4, left), whereas postshock convection in the same stellar model, but without rotation, was not strong enough to drive the shock much farther out than in spherical symmetry [28].

All 2D simulations in Ref. [28], however, were computed with a lateral wedge of about  $90^\circ$ . In case of the rotating model, for example, equatorial symmetry was assumed. This restriction, however, constrains the possible modes of the flow pattern in the convective layer. The calculations in fact show growing power in large structures at later times after bounce, and models with a full  $180^\circ$  grid tend to develop a dominance of the  $l = 1, 2$  modes in connection with global dipolar oscillations of the postshock layer, a phenomenon which is also seen in the three-dimensional case (cf. Refs. [34, 35] and the contribution by Scheck at this meeting). A first 2D simulation with a  $180^\circ$  grid and accurate neutrino transport for a (nonrotating)  $11.2 M_\odot$  star reveals a dramatic difference compared to the  $90^\circ$  run of this progenitor in Ref. [28]: The shock expands continuously with no sign of return until the simulation was stopped at 226 ms post bounce. At that time the expanding shock is highly deformed and has reached a polar radius of more than 600 km (Fig. 4, right). In the  $90^\circ$  simulation the shock was contracting again at that time [28].

### 3 Conclusions

The results reviewed above demonstrate the limits of current state-of-the-art supernova simulations but also indicate the frontiers where ultimate success might be achieved in modeling convectively supported supernova explosions. Rotation of the stellar core, even at a moderate rate, has a strong supporting influence on shock expansion. The same is true for low-mode convection and global nonradial shock instabilities, which are captured by 2D simulations only in case of a full 180° grid and sufficient resolution to follow the amplification of perturbations between shock and neutron star by the “advective-acoustic cycle” [37]. The incompletely known nuclear equation of state adds a component of uncertainty to the problem. Our 1D simulations with different EoSs show interesting and significant differences, but corresponding multi-dimensional simulations with accurate neutrino transport have yet to be done.

### Acknowledgements

We are grateful to K. Nomoto, A. Heger, S. Woosley, and M. Limongi for providing us with their progenitor data. Supercomputer time at the John von Neumann Institute for Computing in Jülich and the Rechenzentrum Garching is acknowledged. This work was supported by the Sonderforschungsbereich 375 “Astroparticle Physics” and the Sonderforschungsbereich/Transregio 7 “Gravitational Wave Astronomy” of the Deutsche Forschungsgemeinschaft.

### References

- [1] M. Rampp and H.-Th. Janka, *A&A* **396** (2002) 361.
- [2] R. Buras et al. (2004), in preparation; R. Buras, PhD Thesis, TU München (2004).
- [3] M. Liebendörfer, M. Rampp, H.-Th. Janka, and A. Mezzacappa, *ApJ*, submitted ([astro-ph/0310662](#)).
- [4] R. Buras, H.-Th. Janka, M.Th. Keil, G. Raffelt, and M. Rampp, *ApJ* **587** (2003) 320.
- [5] J.M. Lattimer and F.D. Swesty, *Nucl. Phys.* **A535** (1991) 331; J.M. Lattimer, C.J. Pethick, D.G. Ravenhall, and D.Q. Lamb, *Nucl. Phys.* **A432** (1985) 646.
- [6] K. Nomoto, *ApJ* **277** (1984) 791; *ApJ* **322** (1987) 206.
- [7] F.S. Kitaura Joyanes, Diploma Thesis, TU München (2003).
- [8] W. Hillebrandt, R.G. Wolff, and K. Nomoto, *A&A* **133** (1984) 175; W. Hillebrandt and R.G. Wolff, in *Nucleosynthesis: Challenges and New Developments*, W.D. Arnett and J.W. Truran (Eds.), Univ. Chicago Press (1985), p. 131.
- [9] R. Mayle and J.R. Wilson, *ApJ* **334** (1988) 909.
- [10] E. Baron, J. Cooperstein, and S. Kahana, *ApJ* **320** (1987) 300.
- [11] S.E. Woosley and E. Baron, *ApJ* **391** (1992) 228.
- [12] C. Fryer, W. Benz, M. Herant, and S.A. Colgate, *ApJ* **516** (1999) 892.
- [13] K. Nomoto and M. Hashimoto, *Phys. Rep.* **163** (1988) 13.
- [14] S.E. Woosley, A. Heger and T.A. Weaver, *Rev. Mod. Phys.* **74** (2002) 1015.
- [15] S.E. Woosley and T.A. Weaver, *ApJS* **101** (1995) 181.
- [16] M. Limongi, O. Straniero, and A. Chieffi, *ApJS* **129** (2000) 625.
- [17] M. Liebendörfer, *et al.*, *ApJS* **150** (2004) 263.

- [18] M. Liebendörfer, *et al.*, Nucl. Phys. **719** (2003) 144c.
- [19] K. Langanke, *et al.*, PRL **90** (2003) 241102.
- [20] A. Heger and S.E. Woosley, <http://www.stellarevolution.org>.
- [21] T.A. Thompson, A. Burrows, and P.A. Pinto, ApJ **592** (2003) 434.
- [22] F.D. Swesty, J.M. Lattimer, and E.S. Myra, ApJ **425** (1994) 195.
- [23] H. Shen, H. Toki, K. Oyamatsu, and K. Sumiyoshi, Nucl. Phys. **A637** (1998) 435; Prog. Theor. Phys. **100** (1998) 1013.
- [24] A. Marek, Diploma Thesis, TU München (2003).
- [25] M. Herant, W. Benz, W.R. Hix, C.L. Fryer, and S.A. Colgate, ApJ **435** (1994) 339.
- [26] A. Burrows, J. Hayes, and B.A. Fryxell, ApJ **450** (1995) 830.
- [27] H.-Th. Janka and E. Müller, A&A **306** (1996) 167.
- [28] R. Buras, M. Rampp, H.-Th. Janka, and K. Kifonidis, PRL **90** (2003) 241101.
- [29] C.L. Fryer, ApJ **522** (1999) 413; C.L. Fryer and A. Heger, ApJ **541** (2000) 1033; C.L. Fryer and M.S. Warren, ApJ **574** (2002) L65; ApJ **601** (2004) 391.
- [30] E. Müller, M. Rampp, R. Buras, and H.-Th. Janka, ApJ **603** (2004) 221.
- [31] A. Heger, S.E. Woosley, N. Langer, and H.C. Spruit, in *Stellar Rotation*, Proc. IAU 215 ([astro-ph/0301374](#)).
- [32] C.D. Ott, A. Burrows, E. Livne, and R. Walder, ApJ **600** (2004) 834.
- [33] K. Kotake, S. Yamada, and K. Sato, ApJ **595** (2003) 304.
- [34] J.M. Blondin, A. Mezzacappa, and C. DeMarino, ApJ **584** (2003) 971.
- [35] L. Scheck, T. Plewa, H.-Th. Janka, K. Kifonidis, and E. Müller, PRL **92** (2004) 011103.
- [36] H.-Th. Janka, R. Buras, K. Kifonidis, A. Marek, and M. Rampp, in *Supernovae (10 Years of SN1993J)*, Proc. IAU Coll. 192 ([astro-ph/0401461](#)).
- [37] T. Foglizzo, A&A **392** (2002) 353; T. Foglizzo and P. Galletti, in *3D Signatures in Stellar Explosions*, Proc. Workshop, Austin, Texas, June 10–13, 2003 ([astro-ph/0308534](#)).